Properties of nanostructured doped ZnO thin films grown by spray pyrolysis technique

© *Sadananda Kumar N.*¶, *Kasturi V. Bangera, G.K. Shivakumar*

Thin Films Laboratory, Department of Physics, National Institute of Technology Karnataka, Surathkal,
575025 Mangalore, India

Aluminium doped zinc oxide thin films are deposited on glass substrate by using spray pyrolysis technique. The X-ray diffraction study of the films revealed that the both the undoped and Al doped ZnO thin films exhibits hexagonal wurtzite structure. The preferred orientation is (002) for undoped and up to 3 at% Al doping, further increase in the doping concentration to 5 at% changes the preferred orientation to (101) direction. The surface morphology of the films studied by scanning electron microscope, reveal marked changes on doping. Optical study indicates that both undoped and Al doped films are transparent in the visible region. The band gap of the films increased from 3.24 to 3.36 eV with increasing Al dopant concentration from 0 to 5 at% respectively. The Al doped films showed an increase in the conductivity by three orders of magnitude with increase in doping concentration. The maximum value of conductivity 106.3 S/cm is achieved for 3 at% Al doped films.

1. Introduction

Zinc oxide (ZnO) is an important wide band gap (3.37 eV) semiconductor material belonging to II−VI group. Due to its properties like wide band gap, high exciton binding energy of 60 meV [1], high optical and electrical properties, it is used in the optoelectronic devices such as solar cells [2], light emitting diodes [3], heat mirrors [4] and thin film transistors [5]. Due to the defects such as oxygen vacancies and zinc interstitials ZnO has conductivity of n-type [6]. The oxygen vacancies and zinc interstitials acts as donors, as excess charge carriers created by them. The formation of carriers by the ionization of zinc interstitials has been acknowledged to be predominant in intrinsic ZnO crystals [7]. To increase the number of charge carriers in ZnO crystals was achieved by thermal [8,9] or by suitable doping process [7,10,11].

In the present study selects aluminium as a dopant. Effects of Al doping on the structural, optical and electrical properties of the film was studied. The various methods such as sputtering [12], physical vapour deposition [13], molecular beam epitaxy [14], metal organic chemical vapour deposition [15], sol gel method [16] and spray pyrolysis technique [17] are employed to deposit the ZnO film. Spray pyrolysis technique was used to prepare the films because it has the advantages of simple, inexpensive, easy-to-dope the elements and helpful for large area surface coating. In this paper we reported the deposition of undoped and Al doped zinc oxide nanostructures on glass substrate using spray pyrolysis technique and the effects of aluminium doping on the surface morphology, structural, electrical and optical properties of the zinc oxide nanostructures.

2. Experimental details

Undoped and Al doped ZnO thin films were deposited on the ultrasonically cleaned glass substrate at $450 \pm 5°$C

using spray pyrolysis technique. Starting solution of 0.05M zinc acetate anhydrous $[Zn(CH_3COO)_2]$ in methanol is used to spray. Aluminium chloride is used as source of dopant $[AlCl_3]$. Atomic % of Al is varied from 0 to 5 by changing the molar ratio in the spray solution. The solution is sprayed by means of glass nozzle on the hotter substrate with a spray rate of 2 ml/min. Air is used as carrier gas and the separations between the nozzle to substrate is fixed at 24 cm to deposit the uniform zinc oxide films.

Thickness of the deposited film was determined using gravimetric method. The films of around 0.6μm thick were used for the present study. The structural characterization of the film was carried out using X-ray diffractometer with Cuk_α radiation of wavelength $\lambda = 1.5418$ Å. The influence of Al doping concentration on the structure of ZnO thin films was investigated. The crystallite size was calculated from the Scherrer's formula. Scanning electron microscope (SEM) was used to study the surface morphology of the films. The composition of undoped and Al doped ZnO thin film was studied using energy dispersive analysis of X-ray (EDAX). The optical properties of undoped and Al doped films were studied using UV-Visible spectrophotometer. The electrical properties of the films were determined with the Keithley multimeter and source meter. The Hall measurements of the Al doped ZnO films were determined by using Van der Pauw's method in a magnetic field strength of 0.45 T at room temperature.

3. Results and discussions

3.1. Structural and morphological characterization

XRD pattern of undoped and Al doped ZnO thin films were shown in the Fig. 1. The calculated values of d_{hkl} are compared with the standard, which confirms that both undoped and Al doped ZnO thin films are exhibits poly-crystalline hexagonal wurtzite structure. The preferential orientation of (002) direction retains up to 3 at% Al doped films, which changes to (101) direction for 5 at% Al doped

¶ E-mail: sadanthara@gmail.com

films. Increase in the doping concentration reduces the (002) peak intensity suggesting that deterioration of the film crystallinity. The slight shift in the (002) peak position was observed with increasing doping concentration.

This confirms the replacement of Zn^{2+} ions by Al^{3+} ions substitutionally in the ZnO lattice. However there no peak corresponding to aluminium or aluminium related phases was detected in the XRD pattern.

The crystallite size of the undoped and Al doped ZnO thin films are estimated from the high intensity peak of XRD pattern using the Scherrer's formula [18]

$$D_{hkl} = \frac{0.9\lambda}{\beta \cos\theta}, \qquad (1)$$

where λ is the wavelength of X-ray's, β is full width at half maximum. θ is Bragg angle. Crystallite size of the
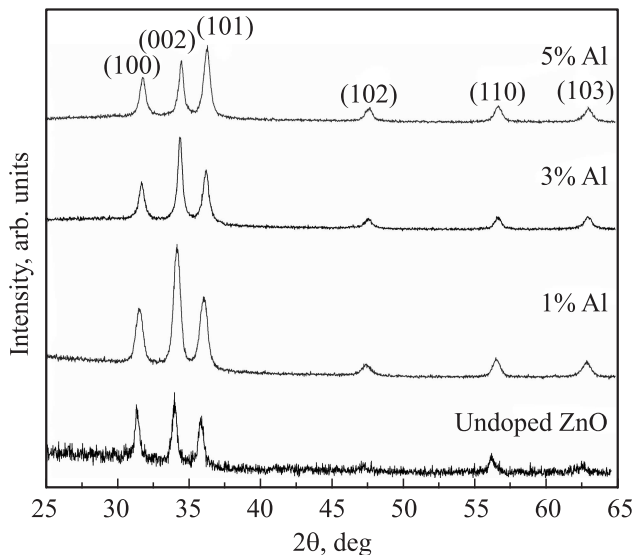

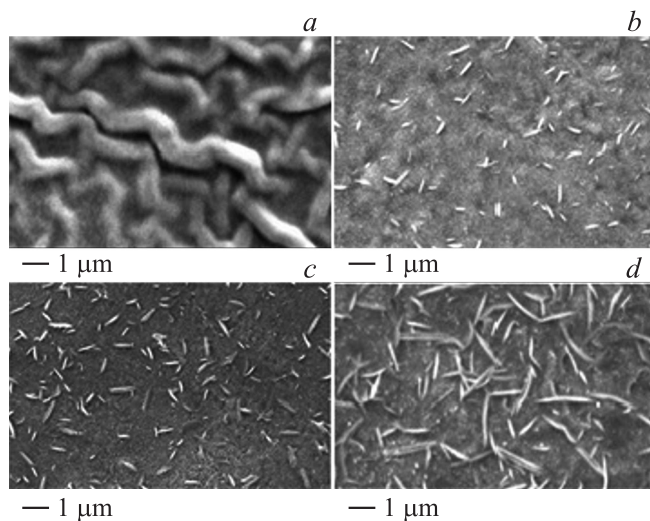**Figure 1.** XRD pattern of undoped and Al doped ZnO thin films.

Figure 2. SEM image of (*a*) undoped ZnO film, (*b*) 1 at%, (*c*) 3 at% and (*d*) 5 at% Al doped ZnO films.

Table 1. XRD data of undoped and Al doped ZnO thin films

Al, at%	Orientation	D, nm	a, Å	c, Å
0	(002)	13.53	3.27	5.24
1	(002)	15.63	3.24	5.23
3	(002)	23.28	3.23	5.22
5	(101)	21.66	3.23	5.21

films found to be increased with increase in the doping concentration upto 3 at% Al doping. Further increase in the doping concentration decreases the crystallites size. The calculated values of crystallite size are listed in the Table 1. The lattice parameters a and c of undoped and Al doped ZnO thin films were calculated using the formula [19]

$$\frac{1}{d^2} = \frac{4\left(h^2 + k^2 + hk\right)}{3a^2} + \frac{l^2}{c^2}. \qquad (2)$$

The lattice parameters were found to be decreased with increasing Al doping concentration. The calculated values of a and c are shown in the Table 1.

The SEM image of undoped and Al doped ZnO thin films are shown in the Fig. 2. The undoped ZnO films show the fiber-like structure with rough surface (Fig. 2, *a*), when the doping concentration increased to 1 at%, fiber like structure disappears and needles like structures were grown on the surface (Fig. 2, *b*). On increasing the Al dopant concentration to 3 at% and above the number of needles and the length of the needles were found to be increased (Fig. 2, *c, d*). The successful incorporation of Al in the ZnO films is confirmed by using EDAX analysis. Also the composition on the needles was analysed using EDAX and it shows the presence of both zinc and aluminium.

3.2. Optical properties

The transmittance spectra of undoped and Al doped ZnO thin films at room temperature are shown in the Fig. 3. Undoped films show the transparency above 77% in the visible region. The maximum transparency of 83% for wavelengths over 550 nm is recorded for 1 at% Al doped ZnO thin films. This increase in the transparency is may be due to the fact that doped films provides more voids than the undoped films, which may reduce the optical scattering. Similar result is observed by Hong-ming Zhou et al. [20] in their Al doped ZnO thin films by sol-gel methods. It is also observed from the Fig. 3 that sharp absorption edge is slightly shifted to lower wavelength region for Al doped films, which confirms the incorporation of Al into the ZnO films. Analytical representations for films optical responses are used to establish a correlation between film nanostructure and optical properties. Changes in optical properties, i.e. broadening and shift of the main electronic transition are related to structure crystallinity and compositional changes [21].

Fig. 4 shows the Tauc's plot of ZnO and Al doped ZnO thin films. According to practical and theoretical results,
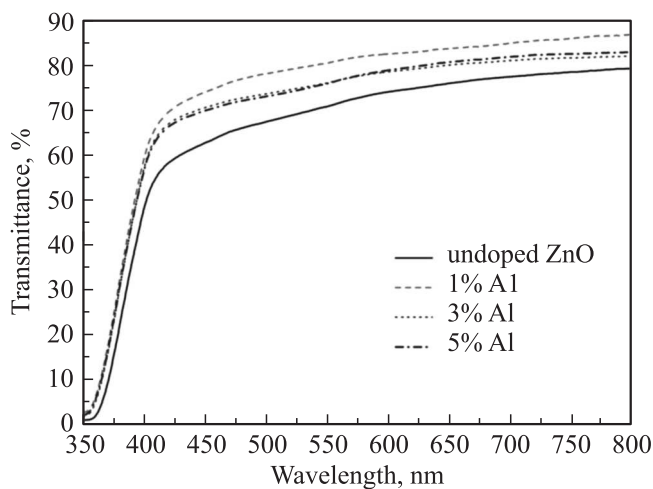
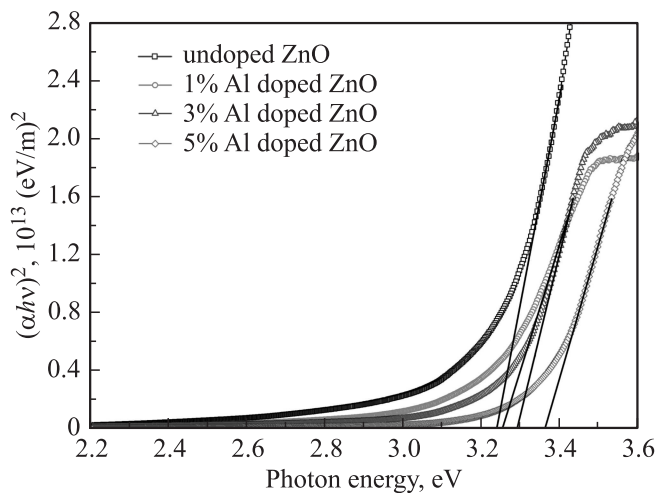**Figure 3.** Transmittance spectra of undoped and Al doped ZnO thin films.

Figure 4. Variation of $(\alpha h\nu)^2$ vs. photon energy of undoped and Al doped ZnO films.

ZnO exhibits direct band to band transitions [22] and the variation of absorption coefficient with photon energy for direct allowed transitions between bands should obey the relation [23]:

$$\alpha h\nu = A(h\nu - E_g)^{1/2}, \qquad (3)$$

where α is the absorption coefficient, $h\nu$ is photon energy, A is constant and E_g is energy band gap. The energy band gap of ZnO and Al doped ZnO thin films can be determined by extrapolating the linear part of the plot $(\alpha h\nu)^2$ vs. photon energy. It is seen that the energy band gap values were increased with increasing Al dopant concentration. The optical band gap of ZnO thin films increased from 3.24 to 3.36 eV with increasing aluminium dopant concentrations from 0 to 5 at% respectively. The increase in the optical band gap is due to the Burstein−Moss effect [24]. This indicates the rise in Fermi level in the conduction band due to increased charge carriers, which leads to broadening of the optical band-gap. According to the reports, energy band

gap of single crystal ZnO is about 3.37 eV [25], which is a greater than calculated band gap value. The observed low value of band gap may be due to the presence of native point defects like zinc interstitials and oxygen vacancies. These point defects create intrinsic defect levels leading to n-type doping. The defect levels exists approximately 0.01−0.05 eV below the conduction band [26]. Urbach energy (E_u) is related to absorption coefficient, α by the equation [27]:

$$\alpha = \alpha_0 \exp(h\nu/E_u), \qquad (4)$$

where α_0 is a constant and E_u represents the disorder in the film network. Calculated E_u, values vary from 253 to 375 meV as the Al doping concentration increased from 0 to 5 at% respectively. Increase in the Urbach energy is due to induced distortion in the material network which arises from difference in the ionic radii of zinc and aluminium. Similar results were obtained for Chouikh et al. [28] in their Bi doped ZnO thin films.

3.3. Electrical Characterization

The Al doped ZnO nanostructures have the advantage of a large surface area, and electronic properties are strongly influenced by surface processes [29]. The Al doped ZnO nanostructures influences to increase in the conductivity of the films by trapping of electrons in the grain boundaries. The grain size of the 3% Al doped ZnO film ($\sim 22\,\text{nm}$) is less than the Debye length ($\sim 30\,\text{nm}$ for nano ZnO) and this indicates that the accumulation of charge carriers in the grain boundary hence electrical conductivity increases [30].

The calculated values of band gap, transmittance, Urbach energy, resistivity and activation energies of undoped and Al doped ZnO thin films are shown in the Table 2. Current−Voltage characteristics of undoped and Al doped ZnO thin films are shown in the Fig. 5. Undoped and Al doped films show linear $I-V$ characteristics, satisfying Ohmic conduction mechanism. The conductivity of undoped ZnO thin film is 0.156 S/cm and it is increased by three orders of magnitude when doped with aluminium. Films doped with 3 at% Al shows high conductivity of 106.3 S/cm. The improved conductivity in Al doped ZnO thin films are due to replacement of Zn^{2+} ions by Al^{3+} ions substitutionally [31]. Addition of small quantity of aluminium contributes more number of free charge carriers in the doped films, therefore conductivity increases. Disorder may produce in the lattice at higher

Table 2. Optical and electrical data of undoped and Al doped ZnO thin films

Al, at%	E_g, eV	T, %	E_u, meV	σ, S · cm^{-1}	E_{a1}, meV	E_{a2}, meV
0	3.24	78	253	0.156	348.0	−
1	3.25	85	305	23.3	181.6	38.8
3	3.29	82	348	106.3	125.2	44.0
5	3.36	83	375	78.60	230.4	63.8

Table 3. Hall measurements data of undoped and Al doped ZnO films

Sample	Resistivity ρ, $\Omega \cdot$ cm	Hall coefficient R_h cm^3/C	Carrier concentration n, cm^{-3}	Mobility μ, cm$^2 \cdot$ V$^{-1} \cdot$ s
Undoped ZnO	6.41	63	$9.92 \cdot 10^{16}$	9.38
1% Al	0.0429	1.147	$5.45 \cdot 10^{18}$	26.72
3% Al	0.0094	0.32	$19.53 \cdot 10^{18}$	34.05
5% Al	0.0127	0.386	$16.19 \cdot 10^{18}$	30.39

doping concentration (5 at%) due to difference in the ionic radius of zinc (0.074 nm) and aluminium (0.055 nm). This enhances the scattering efficiency such as ionized impurity scattering and phonon scattering which intern reduces the conductivity [32]. Further increase in Al doping concentration reduces the conductivity of the films. This decrease in conductivity is may be due to the segregation of excess aluminium in the grain boundary which reduces the conductivity of the films.

The Hall measurements data of the Al doped ZnO films made at room temperature in a magnetic field strength of 0.45 T are shown in the Table 3. The Hall measurements data shows that the increase in the carrier concentration (n) and mobility (μ) of the ZnO films after doping with the trivalent aluminium ions indicates that divalent zinc ion being replacing by trivalent aluminium ions leading to formation of zinc interstitials. It is worth noting that the sheet density does not depend on the Al dopant concentration. The ZnO films prepared with 3 at% Al shows the highest conductivity of 106.3 S/cm with a electron concentration of $19.53 \cdot 10^{18}$ cm^{-3} and a Hall mobility of 34.05 cm$^2 \cdot$ V$^{-1} \cdot$ s^{-1}. The carrier concentration was found to be decreased for 5 at% Al doped films. The reduction in the mobility at higher (5%) Al doping concentration indicates that it is a grain boundary scattering mechanism rather than ionized impurity scattering [33] since the grain size decreased for 5% Al doped films. The reduced
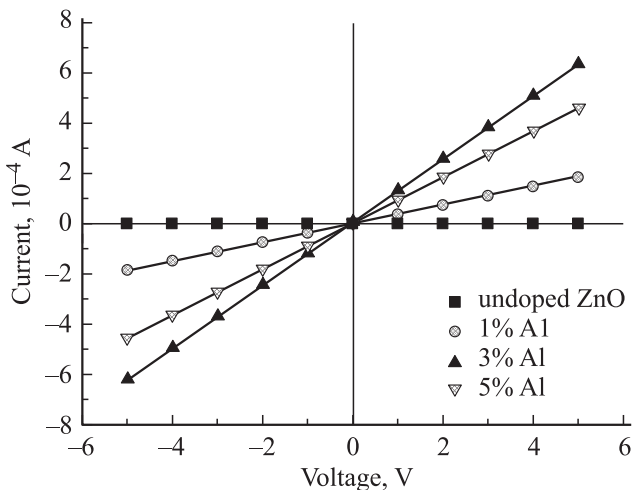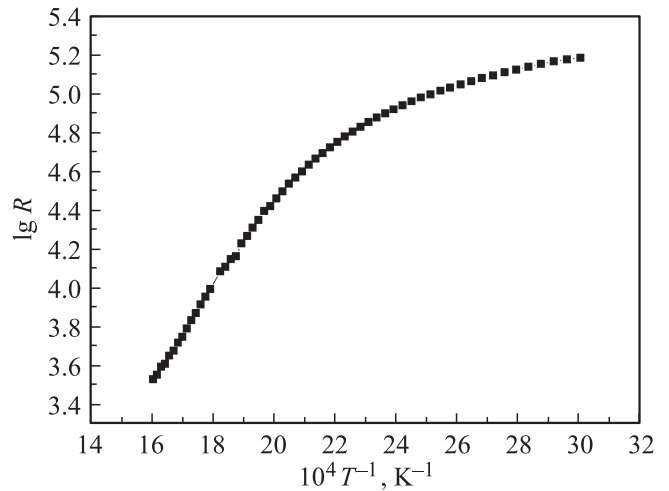
Figure 6. Variation of $\lg R$ with inverse temperature of 3% Al doped ZnO thin films.

doping concentration and mobility explains the decrease in the conductivity of the ZnO films at higher Al doping concentrations.

In the present study activation energies of the undoped and Al doped ZnO films were studied. Fig. 6 shows the variation of $\lg R$ with reciprocal of temperature for the Al doped ZnO thin film. It is observed that resistance increases with increasing temperature indicating semiconducting nature of the films. There are two different linear parts having different slopes were observed for all Al doped ZnO thin films. This indicates that there are two mechanisms for electrical conduction. Similar results were obtained by Jimenez−Gonzalez et al. [34] in their Al doped ZnO films by sol gel method. According to reports the electron concentration in the ZnO films increases by the Al doping and the trapping levels with activation energy less than 55 meV contribute to the electrical conductivity with a very low energy cost.

4. Conclusions

Undoped and Al doped ZnO thin films are deposited by simple and inexpensive spray pyrolysis technique. Effect of Al dopant concentration on the structural, optical and electrical properties have been studied. All the films exhibit polycrystalline hexagonal wurtzite structure with (002)

Figure 5. Current−voltage characteristics of undoped and Al doped ZnO thin films.

preferred orientation. SEM analysis showed the formation of nanostructures. Optical band gap of the films increased with increasing dopant concentration. Transparency of the films in the visible region increased with Al doping. The high conductivity of 106.3 S/cm is obtained for 3 at% doped films. The highly transparent and conductive 3 at% Al doped ZnO thin films can be used as transparent electrodes.

References

[1] D.C. Look. Mater. Sci. Eng. B, **80**, 383−387 (2001).

[2] N. Ohta, D. Ohba, S. Sato, Z. Tang, H. Shimizu 1, H. Shira. Thin Solid Films, **519**, 6920−6927 (2011).

[3] Hong Seong Kang, Jeong Seok Kang, Seong Sik Pang, Eun Sub Shim, Sang Yeol Lee. Mater. Sci. Eng. B, **102**, 313−316 (2003).

[4] Li Gong, Zhizhen Ye, Jianguo Lu, Liping Zhu, Jingyun Huang, Xiuquan Gu, Binghui Zhao. Vacuum, **84**, 947−952 (2010).

[5] Deuk-Hee Lee, Ki-Ho Park, Sangsig Kim, Sang Yeol Lee. Thin Solid Films, **520**, 1160−1164 (2011).

[6] D.C. Look, J.W. Hemsky, J.R. Sizelove. Phys. Lett., **82**, 2552 (1999).

[7] Jin-Hong Lee, Byung-Ok Park. Mater. Sci. Eng. B, **106**, 242−245 (2004).

[8] J.H. Lee, K.H. Ko, B.O. Park. J. Cryst. Growth, **247**, 119 (2003).

[9] P. Nunes, E. Fortunato, R. Martins. Inter. J. Inorg. Mater., **3**, 1125 (2001).

[10] F. Wu , L. Fang, Y.J. Pan, K. Zhou, H.B. Ruan, G.B. Liu, C.Y. Kong. Thin Solid Films, **520**, 703−707 (2011).

[11] P.K. Manoj, Benny Joseph, V.K. Vaidyan, D. Sumangala Devi Amma. Ceram. Intern., **33**, 273−278 (2007).

[12] Wei Gao, Zhengwei Li. Ceram. Intern., **30**, 1155−1159 (2004).

[13] G. Jimenez-Cadena, E. Comini, M. Ferroni, A. Vomiero, G. Sberveglieri. Mater. Chem. Phys., **124**, 694−698 (2010).

[14] K. Ramamoorthy, C. Sanjeeviraja, M. Jayachandran, K. Sankaranarayanan, Pijush Bhattacharya, L.M. Kukreja. J. Cryst. Growth, **226**, 281−286 (2001).

[15] A. Marzouki, A. Lusson, F. Jomard, A. Sayari, P. Galtier, M. Oueslati, V. Sallet. J. Cryst. Growth, **312**, 3063−3068 (2010).

[16] H. Benelmadjat, B. Boudine, O. Halimi, M. Sebais. Opt. Laser Technol., **41**, 630−633 (2009).

[17] A. Chakraborty, T. Mondal, S.K. Bera, S.K. Sen, R. Ghosh, G.K. Paul. Mater. Chem. Phys., **112**, 162−166 (2008).

[18] Chien-Yie Tsay, Hua-Chi Cheng, Yen-Ting Tung, Wei-Hsing Tuan, Chung-Kwei Lin. Thin Sol. Films, **517**, 1032−1036 (2008).

[19] Yasemin Caglar, Seval Aksoya, Saliha Ilican, Mujdat Caglar. Superlat. Microstr., **46**, 469−475 (2009).

[20] Hong-ming Zhou, Dan-qing Yi, Zhi-ming Yu, Lai-rong Xiao, Jian Li. Thin Sol. Films, **515**, 6909−6914 (2007).

[21] Maria Losurdo. Thin Sol. Films, **455−456**, 301−312 (2004).

[22] E. Centinorgu, S. Goldsmith. J. Phys. D: Appl. Phys., **40**, 5220−5236 (2007).

[23] Chien-Yie Tsay, Kai-Shiung Fan, Sih-Han Chen, Chia-Hao Tsai. J. Alloys Comp., **495**, 126−130 (2010).

[24] B.E. Sernelius, K.F. Berggren, Z.C. Jin, I. Hamberg, C.G. Granqvist. Phys. Rev. B **37**, 10 244 (1988).

[25] J.I. Pankove. *Optical Progress in Semiconductors* (Dover, N.Y., 1975).

[26] S.J. Pearton, D.P. Norton, K. Ip, Y.W. Heo, T. Steiner. Prog. Mater. Sci., **50**, 293−340 (2005).

[27] M.V. Kurik. Phys. Status Solidi a, 8, 9 (1971).

[28] F. Chouikh, Y. Beggah, M.S. Aida. J. Mater Sci: Mater Electron, **22**, 499−505 (2011).

[29] L. Schmidt-Mende, J.L. Mac Manus-Driscoll. Materialstoday **10**, 40 (2007).

[30] M. Caglar, S. Ilican, Y. Caglar, F. Yakuphanoglu. Appl. Surf. Sci., **255**, 4491−4496 (2009).

[31] Z.Q. Xu, H. Deng, Y. Li, Q.H. Guo, Y.R. Li. Mater. Res. Bull., **41**, 354−358 (2006).

[32] M. Mizuhashi. Thin Sol. Films, **76**, 97 (1980).

[33] Gil Mo Nam, Myoung Seok Kwon. J. Information Display, **10**, 1 (2009).

[34] A.E. Jimenez-Gonzalez, Jose A. Soto Urueta, R. Suarez-Parra, J. Cryst. Growth, **192**, 430−438 (1998).

Редактор Т.А. Полянская